The Journal of Chemical Physics

RESEARCH ARTICLE | APRIL 24 2023

Phase coexistence implications of violating Newton's third law

Yu-Jen Chiu ; Ahmad K. Omar

J. Chem. Phys. 158, 164903 (2023)
https://doi.org/10.1063/5.0146822

AIP Publishing

The Journal of Chemical Physics ARTICLE scitation.org/journal/jcp

Phase coexistence implications of violating Newton's third law

Cite as: J. Chem. Phys. 158, 164903 (2023); doi: 10.1063/5.0146822
Submitted: 16 February 2023 • Accepted: 17 March 2023 •
Published Online: 24 April 2023

Yu-Jen Chiu[1] and Ahmad K. Omar[1,2,a)]

AFFILIATIONS

[1] Department of Materials Science and Engineering, University of California, Berkeley, California 94720, USA
[2] Materials Sciences Division, Lawrence Berkeley National Laboratory, Berkeley, California 94720, USA

[a)] **Author to whom correspondence should be addressed:** aomar@berkeley.edu

ABSTRACT

Newton's third law, *action* = *reaction*, is a foundational statement of classical mechanics. However, in natural and living systems, this law appears to be routinely violated for constituents interacting in a nonequilibrium environment. Here, we use computer simulations to explore the macroscopic phase behavior implications of breaking microscopic interaction reciprocity for a simple model system. We consider a binary mixture of attractive particles and introduce a parameter that is a continuous measure of the degree to which interaction reciprocity is broken. In the reciprocal limit, the species are indistinguishable, and the system phase separates into domains with distinct densities and identical compositions. Increasing nonreciprocity is found to drive the system to explore a rich assortment of phases, including phases with strong composition asymmetries and three-phase coexistence. Many of the states induced by these forces, including traveling crystals and liquids, have no equilibrium analogs. By mapping the complete phase diagram for this model system and characterizing these unique phases, our findings offer a concrete path forward toward understanding how nonreciprocity shapes the structures found in living systems and how this might be leveraged in the design of synthetic materials.

INTRODUCTION

Living and natural systems across all length scales can appear to violate Newton's third law. A familiar example is the so-called "predator–prey" interaction, whereby one entity (the predator) feels an attractive force toward the other, while the other (the prey) is repelled. These *effective nonreciprocal interactions* can emerge from a host of complex factors and can have far-reaching implications on collective phenomena, phase transitions, and pattern formation. In the living world, examples range from the interactions amongst bacteria[1,2] at the microscale to the dynamics of animal herds[3,4] at the macroscale. Synthetic systems with nonreciprocal interactions have also been increasingly realized, with nonreciprocity emerging in systems as diverse as dusty plasmas,[5–10] colloidal suspensions,[11–14] and even solid metamaterials.[15–17] The understanding of the structure and phases of biological systems and leveraging nonreciprocal interactions in synthetic materials will require a fundamental understanding of both the origins and implications of these effective interactions.

Effective forces acting on particles of interest have long been known to shape the structure and properties of condensed matter systems. These forces emerge from the coarse-graining of degrees of freedom, such as other species present within the system. When the coarse-grained degrees of freedom are in equilibrium, the structure of the effective forces is severely restricted: the one-body forces (e.g., fluctuating Brownian and dissipative forces acting on the solute upon coarse-graining a molecular solvent) must satisfy the fluctuation–dissipation theorem (FDT) and many-body forces (e.g., the pairwise depletion force between larger solutes upon coarse-graining smaller solutes) must be conservative and consistent with Newton's third law.[18–22]

Coarse-graining degrees of freedom that are out of equilibrium unlocks a new range of possibilities. In a nonequilibrium environment, one-body forces need not satisfy FDT with these "active" forces, resulting in novel phase transitions and collective phenomena.[23,24] A driven environment may also generate effective *nonreciprocal* many-body forces.[25–34] The consequences of violating interaction reciprocity on phase behavior remain unclear (especially in comparison to those of one-body active forces) and have motivated the development of a variety of theoretical perspectives.[27–32,34]

In this article, we explore the consequences of violating Newton's third law on the phase behavior of a model system where noncreciprocity can be continuously tuned, defining an additional axis on the phase diagram. Increasing nonreciprocity not only leads to exotic states of coexistence, but may also *stabilize* homogeneous states resembling active fluids. Our findings thus reveal that nonreciprocal interactions may impact the phase behavior in new and unexpected ways and constitute an important step forward toward the development of a multicomponent nonequilibrium coexistence theory.

MODEL SYSTEM

Elucidating the influence of nonreciprocal interactions on material phase behavior requires a model system in which the degree of nonreciprocity can be continuously varied. We consider a binary mixture of particles of species L and G with the pairwise force exerted on particle i by particle j taking the following form:[9,27,35,36]

$$\mathbf{F}_{ij}(\mathbf{r}) = \mathbf{F}^{\mathrm{C}}_{ij}(\mathbf{r}) \times \begin{cases} [1-\Delta(r)], & ij \in LG, \\ [1+\Delta(r)], & ij \in GL, \\ 1, & ij \in LL \text{ or } GG, \end{cases} \tag{1}$$

where $\mathbf{r}$ is the interparticle distance vector (with magnitude r), $\mathbf{F}^{\mathrm{C}}_{ij}(\mathbf{r})$ is a *conservative* interaction force satisfying Newton's third law $\left(\text{i.e., } \mathbf{F}^{\mathrm{C}}_{ij} + \mathbf{F}^{\mathrm{C}}_{ji} = \mathbf{0}\right)$, and $\Delta(r)$ is a nonreciprocity function. Interactions between particles of similar species are entirely reciprocal $\left(\mathbf{F}_{ij} = \mathbf{F}^{\mathrm{C}}_{ij}\right)$, while interspecies interactions exhibit both reciprocal $\mathbf{F}^{\mathrm{R}}_{ij} = \mathbf{F}^{\mathrm{C}}_{ij}$ and nonreciprocal $\mathbf{F}^{\mathrm{NR}}_{ij} = \pm\Delta \times \mathbf{F}^{\mathrm{C}}_{ij}$ contributions, with $\mathbf{F}_{ij} = \mathbf{F}^{\mathrm{R}}_{ij} + \mathbf{F}^{\mathrm{NR}}_{ij}$. Consider $ij \in LG$: The sum of this pair interaction will result in a net force (violating Newton's third law), with $\mathbf{F}_{ij} + \mathbf{F}_{ji} = 2\mathbf{F}^{\mathrm{NR}}_{ij} = 2\Delta\mathbf{F}^{\mathrm{C}}_{ij}$. This resulting net force $\mathbf{F}^{\mathrm{NR}}_{\mathrm{net}} = 2\mathbf{F}^{\mathrm{NR}}_{ij}$ [see Fig. 1(a)] may be thought of as an internally generated active force that entirely depends on particle configurations and the nonreciprocity function $\Delta(r)$. For simplicity, we consider a step nonreciprocity function $\Delta(r) = \Delta\Theta(r - d_{\mathrm{rec}})$ such that interactions between particles are entirely reciprocal for separation distances less than a reciprocity diameter, d_{rec}, and have a constant degree of nonreciprocity Δ for distances greater than d_{rec}. This model now allows us to continuously depart from the equilibrium limit $(\Delta = 0)$ and isolate the precise role of the violation of interaction reciprocity on a system's phase diagram. In this sense, this model represents a minimal system, in which detailed balance is broken on a *two-body* level, joining a family of simple models in which detailed-balance is broken with a single parameter.[24,37–39]

Figure 1(a) illustrates the qualitatively distinct interaction regimes controlled by Δ. Departures from $\Delta = 0$ break interaction reciprocity, resulting in forces that are no longer conservative and a nonequilibrium distribution of microstates. For $0 < \Delta < 1$, while the magnitude of the force is different for each species, the forces continue to oppose each other: repulsive (attractive) interactions will continue to be repulsive (attractive). However, for $\Delta > 1$, the nonreciprocity results in forces that no longer oppose each other: a particle exerting a repulsive (attractive) force will itself experience an attractive (repulsive) force [see Fig. 1(a)]. This is the so-called "predator–prey" interaction that appears in nature. While this might lead one to conclude that $\Delta = 1$ is a significant dynamical point from the individual particle perspective, from the standpoint of the *particle pair,* this point is not unique. The net nonreciprocal force between the particle pair [see Fig. 1(a)] linearly grows with increasing Δ: there is nothing to distinguish $\Delta = 1$.

Our aim is to identify how nonreciprocity shapes the structural and dynamical landscape of a simple model system. To this end, we take our conservative force $\mathbf{F}^{C}$ to result from Lennard-Jones (LJ) interactions (with a cutoff distance of 2.5σ), introducing the LJ energy (ε) and length (σ) scales. The reciprocal diameter is set to $d_{\mathrm{rec}} = 2^{1/6}\sigma$ such that all particle pairs experience strictly reciprocal repulsion within separation distances of d_{rec}. The resulting pair interaction forces are shown in Fig. 5 in the Appendix. The particle dynamics follow the overdamped Langevin equation (see the Appendix), which imparts an ideal translational diffusivity $D_T = k_BT/\zeta$ (introducing our system timescale $\tau = \sigma^2/D_T$), where k_BT is the thermal energy and ζ is the translational drag coefficient. Our system state is, thus, fully described by four parameters: the degree of nonreciprocity Δ, the global volume fraction $\phi = (\rho_L + \rho_G)\pi(d_{\mathrm{rec}})^3/6$ (where ρ_L and ρ_G are the number densities of species L and G, respectively), the global composition $\chi = \rho_G/(\rho_L + \rho_G)$, and the ratio of the interaction energy to the thermal energy ε/k_BT. In this work, we fix $\chi = 0.5$ and $\varepsilon/k_BT = 2.0$, and systematically sweep ϕ and Δ. All simulations were conducted with 50 000 particles using `HOOMD-blue`.[40]

PHASE DIAGRAM

Figure 1(b) displays the phase diagram obtained from extensive computer simulations. For finite nonreciprocity, the system is out of equilibrium, and, while there has been recent progress in the sampling of driven systems,[41–49] we address questions of global stability by conducting a number of long-time simulations with distinct initial configurations, as detailed in the supplementary material.

STATIONARY PHASE TRANSITIONS

In the reciprocal limit $\Delta = 0$, there is no distinction between L and G particles. The stationary state corresponds to that of a single-component attractive Lennard-Jones system at $\varepsilon/k_BT = 2.0$. While it has been established[50] that the thermodynamic ground state for this system is crystal (fcc)–fluid coexistence, observing this state requires an exceedingly rare fluctuation, to generate the critical nuclei necessary for crystal growth. A long-lived (metastable) liquid–gas coexistence is, instead, observed for all densities examined in this work with $\Delta = 0$.

Small departures from the reciprocal limit $(0 < \Delta \leq 0.15)$ continue to result in liquid–gas coexistence with similar (slightly reduced) coexisting densities [see Fig. 2(a)]. However, a composition asymmetry between the phases is now generated, as shown in Fig. 2(b). For small Δ, it may be permissible to assume that the system remains in a local equilibrium with modified interaction potentials between particle pairs. However, a composition distinction between phases in a symmetric mixture would require difference in the modified LL and GG interaction energies. As nonreciprocity leaves interactions between like species unaltered, systems with weak nonreciprocal forces cannot be mapped to equilibrium with modified interaction energies.

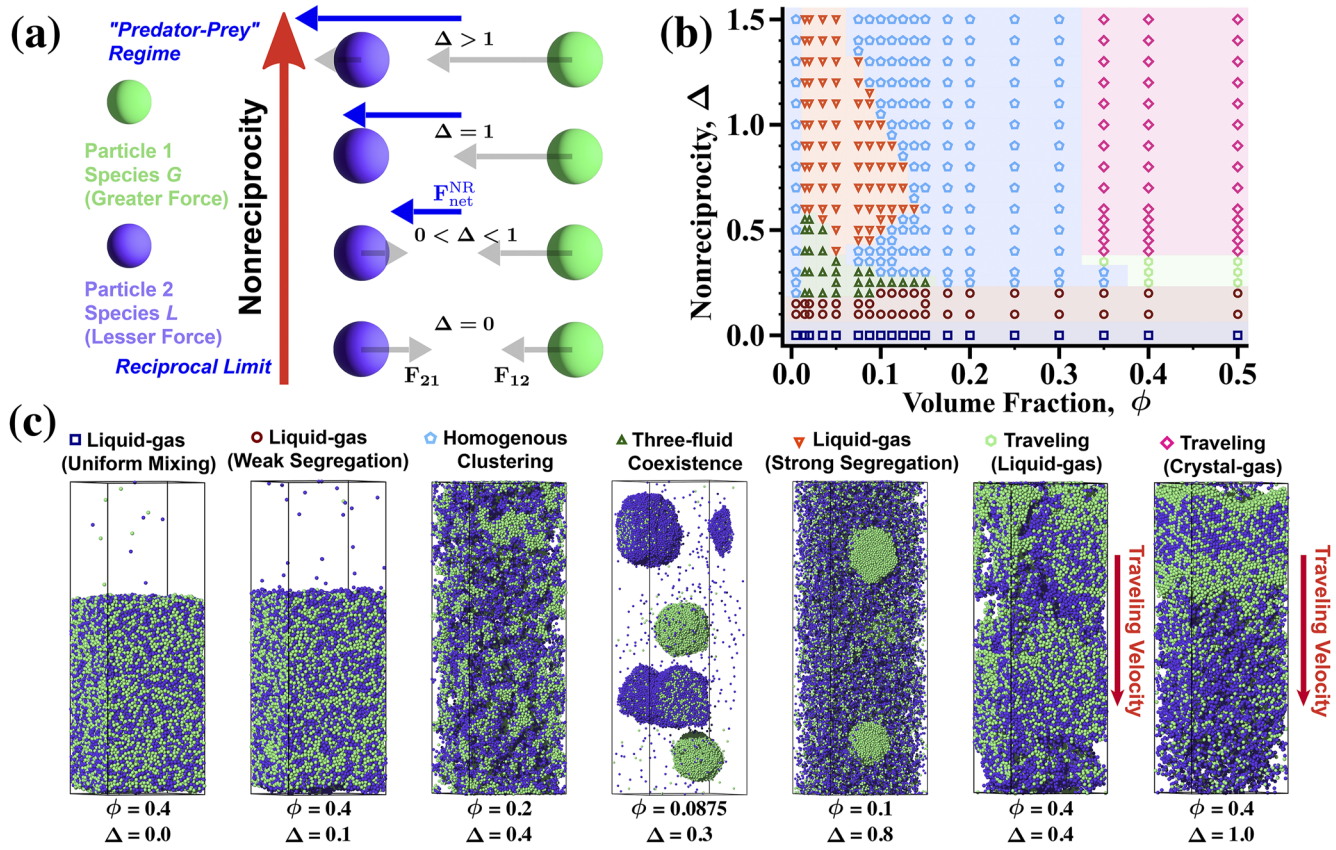

FIG. 1. (a) Schematic of pairwise nonreciprocal interactions between species *L* and *G*. (b) Phase diagram in the density–nonreciprocity plane with $\varepsilon/k_BT = 2.0$ and $\chi = 0.5$, with $\phi \in [0.005, 0.5]$, $\Delta \in [0, 1.5]$. (c) Representative snapshots of each of the seven distinct regions of the phase diagram.

An alternative intriguing possibility exists for this weak species segregation, in which, for small Δ, rather than mapping the system to an equilibrium system with modified interactions, we consider the effective temperatures of each species to slightly deviate from the bath temperature and with $(T_L \neq T_G)$. The statistical mechanics of systems with particles in contact with different heat baths is considerably simpler than a full treatment of nonreciprocity. In fact, this perspective was found to hold exactly in the limit of small nonreciprocity for certain model systems.[27] However, its general applicability to nonreciprocal systems remains to be determined.

In scenarios with species of different temperatures, particles with a higher effective temperature are entropically driven to enrich

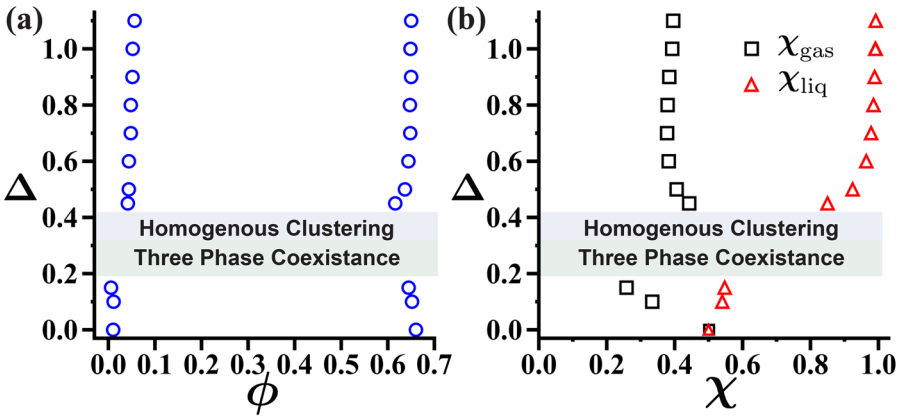

FIG. 2. Nonreciprocity dependence of coexisting (a) densities and (b) compositions for states of two-phase coexistence with $\phi = 0.0875$.

the dilute phase.[51] Our simulation results (Fig. 2) show that particles of species L are biased toward the gaseous phases, suggesting $T_L > T_G$ if this perspective holds. However, there is little evidence to suggest that $T_L > T_G$, as the self- diffusion of G is always greater than that of L [see Fig. 3(b)]. Attempting to define the effective temperature with a Stokes–Einstein relation (i.e., $k_B T_{L/G} = D^{\text{self}}_{L/G}\zeta^{\text{eff}}$, where ζ^{eff} is an effective translational drag coefficient, assumed to be identical for each species) would lead to the interpretation that $T_G > T_L (> T)$. We, thus, conclude that even for the small values of nonreciprocity examined here, effective equilibrium and effective temperature ideas are not sufficient to describe the observed phase behavior.

Increasing the nonreciprocity beyond $\Delta > 0.15$ results in a multitude of states, depending on the overall volume fraction. For a broad range of intermediate densities $(0.15 < \phi < 0.35)$, the system is globally homogeneous (i.e., there is no phase separation). This broad region of intermediate densities at which no phase transitions occur $(0.15 < \phi < 0.35)$ is not the only region of homogeneity. For $\Delta \geq 0.2$, we, indeed, find the system to be homogeneous at the lowest concentration $(\phi = 0.005)$ shown in the phase diagram presented in Fig. 1(b), while systems with $\Delta < 0.2$ are phase separated. It is interesting that even at these low concentrations, the system state remains Δ dependent. In the low density limit, as $\phi \to 0$, this Δ dependence must vanish, as interactions become negligible and the system is indistinguishable from an ideal gas with temperature $k_B T$.

In this broad region of homogeneity at intermediate densities, the system consists of clusters of finite spatial extent. Each cluster is typically enriched in either L or G, and as a result, the system appears to be microphase separated, particularly at smaller values of Δ [cf., Fig. 1(c)]. We characterize the extent of species segregation by computing the partial static structure factors provided in the supplementary material. The correlation lengths for density fluctuations of species L and G, ξ_L and ξ_G, respectively, are extracted from the structure factor and shown in Fig. 3(a). With increasing Δ, we find a monotonic reduction in these correlation lengths: increasing nonreciprocity homogenizes the system at these densities. We note that the divergence of both ξ_L and ξ_G as $\Delta \to 0.2$ is anticipated, as the phase-separated regime is approached in this limit.

What is more, the dramatic alteration to the system's structural properties is accompanied by a commensurate change in the species' self-diffusivity [see Fig. 3(b)]. The diffusion constant in the absence of any interactions is the ideal Stokes–Einstein translational diffusivity, $D_T = k_B T/\zeta$, imparted on the particles by the Langevin bath. In the case of passive systems with purely reciprocal interactions, D_T serves as an upper bound for the self-diffusion constant, with $D^{\text{self}} \leq D_T$. Furthermore, if a Stokes–Einstein relation holds, $D^{\text{self}} = k_B T/\zeta^{\text{eff}}$, where $\zeta^{\text{eff}} \geq \zeta$. Upon increasing Δ, the self-diffusivities of both species increase significantly and even *exceed the ideal diffusivity* for $\Delta \gtrsim 0.6$.

We can determine the precise origins of this enhanced diffusion using the Green–Kubo relation for self-diffusion[52] and leveraging the substitution of forces for velocities permitted by overdamped dynamics. Composition fluctuations about a tagged particle [see Fig. 3(c)] generate instantaneous nonreciprocal forces that act to increase the diffusivity (similar to a one-body active force), and the system resembles an active fluid. However, this contribution is found to be relatively independent of Δ, as detailed in the supplementary material. The origin of the dramatic increase in particle diffusivity with Δ is, in fact, found to be the result of the diminishing magnitude of a number of force correlations that reduce particle mobility. Increased nonreciprocal forcing induces profound structural changes that have a clear dynamical consequence: the breakup of segregated microphases reduces the effective particle friction. The diminished friction with increasing Δ, coupled with the direct contribution of nonreciprocal forcing to particle diffusion, is what allows the system to exceed the ideal diffusion.

At volume fractions between regions of global homogeneity [i.e., $0.005 < \phi \leq 0.15$], nonreciprocity introduces a variety of possible stationary states. Appreciable values of nonreciprocity $(0.2 \leq \Delta \leq 0.55)$ results in a state of *three-phase coexistence*, as

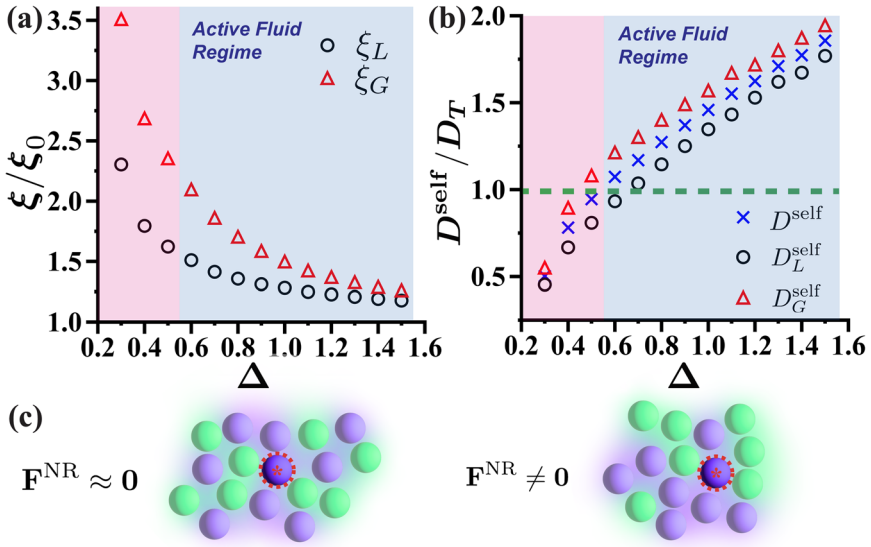

FIG. 3. Nonreciprocity dependence of the (a) correlation lengths [normalized by the ideal gas value ξ_0 (see the Appendix)] and (b) self-diffusivities for $\phi = 0.2$ and $\Delta \geq 0.3$. Shaded regions highlight the active fluid regime ($D^{\text{self}} > D_T$). (c) Fluctuations of the local composition environment of a tagged particle control nonreciprocal forcing.

shown in Fig. 1(b). The three coexisting fluids consist of two high-density, spherical liquid phases,[53] each nearly pure in species L or G, and a dilute phase with a relatively equal amount of each species. In contrast to nonreciprocal two-phase coexistence, the observed densities and compositions may more readily be mapped to an equilibrium analog. In equilibrium, reducing the magnitude of inter-species attraction, i.e., $\varepsilon_{LG} < \varepsilon$, can generate a state of three-phase coexistence, not dissimilar to what we observe here, as detailed in the supplementary material.

Further increasing Δ will result in a return to two-fluid coexistence, with densities similar to those seen at low nonreciprocity [see Fig. 2(a)]. However, unlike lower values of nonreciprocity, there is a sharp composition contrast between the coexisting fluids, as shown in Fig. 2(b). Intriguingly, the dense fluid [again, adopting a spherical morphology, see Fig. 1(c)] is nearly entirely comprised of species G. Preparing a system seeded with a liquid droplet, purely of species L, in this two-phase region of the phase diagram again results in the nucleation and growth of a liquid G droplet—dense liquids of G appear to be the preferred state. In single- component, nonequilibrium systems, interfacial mechanics uniquely determine the coexisting densities.[37,54] While this remains to be generalized to multicomponent systems, the interfacial nonreciprocal forces result in a pure G liquid phase coexisting with a dilute mixture as the mechanically stable state of coexistence.

With increasing nonreciprocity, this region of two-phase coexistence, with strong species segregation, is found to narrow, while the stable homogeneous region of the phase diagram expands [see Fig. 1(b)]. At the highest value of nonreciprocity reported here, the phase diagram has four distinct regions. Beginning at the lowest density, with increasing ϕ, we move from the homogeneous "ideal gas" regime to a two-fluid coexistence, followed by a broad regime of homogeneity. Further increasing the density beyond $\phi \geq 0.35$ results in a traveling state—a dynamical transition that we now discuss.

TRAVELING STATES

At high ϕ, performing the long-time average results in density and composition profiles that resemble traditional states of two-phase coexistence. Intriguingly, at these high concentrations and with increasing nonreciprocity, the dense phase undergoes an ordering transition, with the emergence of an fcc crystal, quantified with the Steinhardt–Nelson–Ronchetti order parameter, measuring 12-fold rotational symmetry, q_{12} (see the Appendix).[55] Typical density and q_{12} profiles are shown in Fig. 4(a), with z being the direction normal to the interface. Did the mobility imparted by nonreciprocal forces allow the system to surmount the nucleation barrier or is nonreciprocity itself driving this ordering transition? We leave interrogating these questions for a future study, but recent work on active order–disorder transitions[56] suggests that nonequilibrium forcing can entirely reshape the crystallization landscape.

While the long-time averages of these states appear consistent with a stationary two-phase coexistence scenario, careful examination of the low-density region reveals a kink in its density profile, suggesting that this is not a typical state of coexistence between two homogeneous phases. Indeed, observing the system dynamics reveals the emergence of a traveling state, defined by ballistic center-of-mass motion [see Fig. 1(c) and the supplementary material]. This density gradient generates an asymmetry that drives a persistent center-of-mass velocity: the coexisting domains appear to chase each other.

These *traveling states* occur for both liquid–gas and crystal–fluid coexistence, depending on the degree of nonreciprocity [see Fig. 1(b)]. Over a time period τ_{ts}, the direction of the low-density phases' density gradient reverses, and with it, so too does the center-of-mass velocity v_{com}. These dynamics are well-described by a simple oscillatory form $v_{com}(t) = v_{ts}\sin(2\pi t/\tau_{ts})$. Figure 4(b) reveals that while the velocity increases nearly linearly with nonreciprocity, there is a marked decrease in the period.[57] That the velocity scales nearly linearly with Δ is perhaps indicative that the traveling speed simply scales with the magnitude of the nonreciprocal forcing, while the oscillation period is dictated by the timescale for the reorganization of the density gradient. The enhanced mobility with increasing Δ [cf., Fig. 3(b)] likely drives the marked reduction in the gradient reorganization time, generating the observed rapid oscillation frequency at high nonreciprocity.

The density gradient, which drives the traveling state, is also accompanied by a composition gradient: the velocity direction is normal to the interface enriched in G [see Fig. 1(c) and the supplementary material, movies]. These traveling states thus appear to be a version of the "predator–prey" interaction, with the G enriched regions chasing the G depleted domains. It is important to

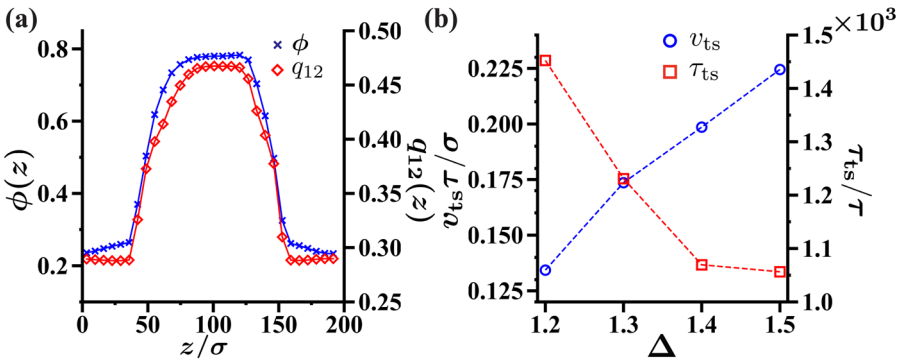

FIG. 4. Traveling crystal (a) long time-averaged ϕ and q_{12} profiles (averaging time $\gg \tau_{ts}$) with ($\Delta = 1.5, \phi = 0.5$) and (b) Δ dependence of the traveling state dynamics for $\phi = 0.5$.

note that traveling states do not require nonreciprocal interactions. Mixtures of active and passive particles,[58–61] interacting with purely reciprocal interactions, can also exhibit such states.[29,34,59,60]

What determines the onset of these dynamical states is the mutual diffusion coefficient tensor $D_{\alpha\beta}$, the elements of which describe how a diffusive flux of species α emerges from a density gradient in species β.[62] Linear stability analysis using the species mass conservation equations results in stability criteria purely in terms of the eigenvalues of $D_{\alpha\beta}$. The traveling phases may emerge when the eigenvalues have imaginary components.[29,30,32,34,60] Constructing the stability diagram for this system will thus require a model for the diffusion tensor. The mutual diffusion coefficients have been analytically computed for some active–passive mixtures,[60] beginning from the evolution equation for the distribution of microscopic configurations for those systems. A general microscopic expression for the mutual diffusion tensor for mixtures with nonreciprocal interactions is the subject of ongoing work, as it will be necessary for the prediction of traveling states from first principles. While $D_{\alpha\beta}$ is crucial for determining stability criteria, predicting the properties of the stable states (e.g., the density and composition of phases) will require additional considerations.

CONCLUSIONS

Nonreciprocity is a generic feature of living and natural systems and is increasingly used as a means to alter the structure and dynamics of synthetic materials across a multitude of length scales. Recent works have sought to generalize statistical mechanics and the theory of dynamical systems to account for nonreciprocity,[27–32,34] however the theory for multicomponent nonequilibrium coexistence remains an outstanding challenge. Here, we have presented a minimal model that illustrates the versatility of nonreciprocity as an added dimension to a system's phase diagram and found that it generates a wealth of stationary and dynamical phase transitions. This added dimension to the phase diagram allows a simple two-component system to access states of three-fluid coexistence, liquid-liquid phase separation with strong species segregation, and traveling crystal phases. The minimal system presented here may thus serve as an ideal model for the development of the nonequilibrium statistical mechanics of mixtures.

SUPPLEMENTARY MATERIAL

See the supplementary material, which includes Refs. 51, 52, and 63–65, for additional simulation and calculation details, as well as simulation movies.

ACKNOWLEDGMENTS

Y.-J.C. acknowledges support from the UC Berkeley College of Engineering Jane Lewis Fellowship. A.K.O. was supported by the Laboratory Directed Research and Development Program of Lawrence Berkeley National Laboratory under U.S. Department of Energy Contract No. DE-AC02-05CH11231 and the UC Berkeley College of Engineering. This research used the Savio computational cluster resource provided by the Berkeley Research Computing program.

AUTHOR DECLARATIONS

Conflict of Interest

The authors have no conflicts to disclose.

Author Contributions

Yu-Jen Chiu: Conceptualization (equal); Writing – original draft (equal); Writing – review & editing (equal). **Ahmad K. Omar**: Conceptualization (equal); Writing – original draft (equal); Writing – review & editing (equal).

DATA AVAILABILITY

The data that support the findings of this study are available from the corresponding author upon reasonable request.

APPENDIX: SIMULATION AND CALCULATION DETAILS

The interaction reciprocity in our simulations is adjusted with a single scalar parameter, Δ. All interactions within the reciprocity diameter $d_{\text{rec}} = 2^{1/6}\sigma$ are reciprocal, and are generally nonreciprocal for interparticle separations greater than d_{rec} for interspecies pairs. Figure 5 plots the pairwise forces resulting from our choice of the reciprocity diameter and the use of a Lennard-Jones potential. The sign convention is chosen such that positive forces are repulsive and negative forces are attractive. The emergence of nonreciprocity is evident with increasing Δ.

Particle dynamics are taken to follow the overdamped Langevin equation

$$\dot{\mathbf{x}}_i = \frac{1}{\zeta}\sum_{i\neq j}\mathbf{F}_{ij}(r;t) + \mathbf{v}_i^s(t), \tag{A1}$$

where $\dot{\mathbf{x}}_i$ is the velocity of the ith particle, $\mathbf{v}_i^s(t)$ is a stochastic velocity with a mean of $\langle \mathbf{v}_i^s(t)\rangle = \mathbf{0}$ and variance of $\langle \mathbf{v}_i^s(t)\mathbf{v}_j^s(t')\rangle = 2D_T\delta_{ij}\delta(t-t')\mathbf{I}$, D_T is the translational diffusion coefficient (defining the thermal energy scale $k_BT = \zeta D_T$), $\delta(t-t')$ is the Dirac delta function, and $\mathbf{I}$ is the identity tensor. These conservative forces are cut off at 2.5σ, capturing the attractive portion of the LJ potential, and we set $d_{\text{rec}} = 2^{1/6}\sigma$ such that all particle pairs experience reciprocal repulsion within separation distances of d_{rec}. All points sampled in the phase diagram are initialized with random initial conditions generated with `Packmol`[63] and are run for a duration of 5000τ. Points close to the phase boundary are examined with different initial conditions to assess global stability, as detailed in the supplementary material.

Periodic boundary conditions are employed in all directions, and rectangular box geometries are used to orient the interface of coexisting domains. The relative box dimensions for all simulations have a ratio 1:1:3. In the case of traveling states that consist of spatial gradients over large length scales, we conduct additional simulations with relative box dimensions 1:1:10. This elongated geometry better

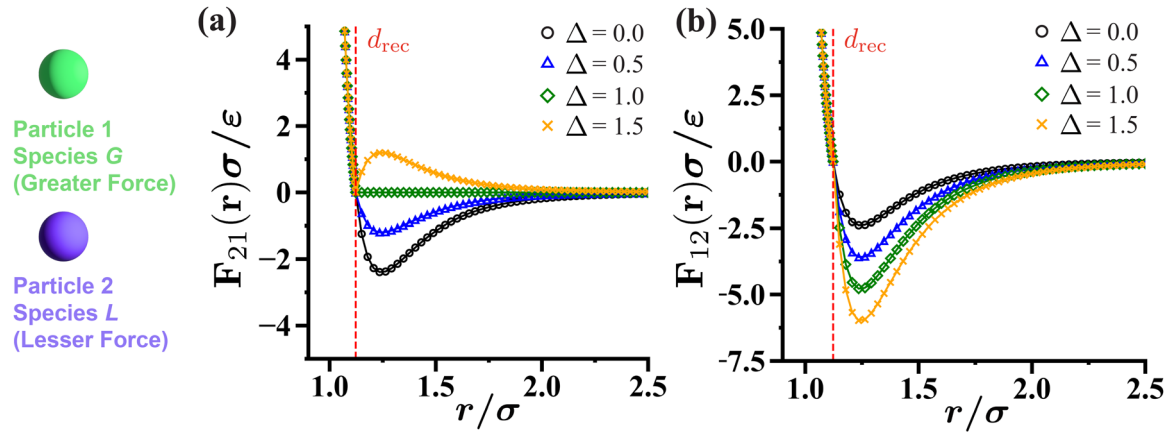

FIG. 5. Δ dependence of the pair interaction force acting on (a) a particle of species *L* by a particle of species *G* and (b) a particle of species *G* by a particle of species *L*.

allows for visualization and characterization of the spatial gradients present in the traveling states.

The correlation lengths presented in Fig. 3(a) are taken to be the inverse of the first moment of the static structure factor

$$\xi_\alpha = \frac{\int_{k_{\min}}^{k^*} S_{\alpha\alpha}(k)dk}{\int_{k_{\min}}^{k^*} kS_{\alpha\alpha}(k)dk}, \tag{A2}$$

where k^* is the magnitude of the wave vector corresponding to the reciprocity diameter and $k_{\min}$ corresponds to the largest possible wavelength, set by the simulation box size. The partial static structure factors $S_{\alpha\beta}$ are computed with the Fourier transform of particle coordination for species α and β. We focus on *intraspecies* density correlations (i.e., $\alpha = \beta$) with $S_{\alpha\alpha}$, taking the following form:

$$S_{\alpha\alpha}(\mathbf{k}) = \frac{1}{N_\alpha}\left\langle\left|\sum_{j=1}^{N_\alpha} \exp\left(i\mathbf{k}\cdot\mathbf{x}_j\right)\right|^2\right\rangle, \tag{A3}$$

where N_α is the total number of particles of species α. For the isotropic systems considered here, $S_{\alpha\alpha}(k)$ depends only on the magnitude of the wave vector $k = |\mathbf{k}|$. Species correlation is normalized by $\xi_0 = \frac{\int_{k_{\min}}^{k^*} S_{\text{ideal}}(k)dk}{\int_{k_{\min}}^{k^*} kS_{\text{ideal}}(k)dk}$, where $S_{\text{ideal}}(k) = 1$ is the ideal gas static structure factor.

The Steinhardt–Nelson–Ronchetti order parameter q_{12} computed in Fig. 4(a) is defined as

$$q_l(i) = \left(\frac{4\pi}{2l+1}\sum_{m=-l}^{l}|\langle q_{lm}\rangle|^2\right)^{1/2}, \tag{A4}$$

where q_{lm} is the average spherical harmonics of the bond angles formed between particle i and its nearest neighbors.[55] By taking $l = 12$, we can quantify the presence of twelve-fold rotational symmetry in the local structure around a tagged particle, with $q_{12} \approx 0.6$ corresponding to a perfect fcc arrangement and $q_{12} \approx 0.3$ for a disordered fluid. We use q_{12} to distinguish between traveling liquid–gas and traveling crystal–gas scenarios.

REFERENCES

[1] R. A. Long and F. Azam, Appl. Environ. Microbiol. **67**, 4975 (2001).
[2] A. Czirók, E. Ben-Jacob, I. Cohen, and T. Vicsek, Phys. Rev. E **54**, 1791 (1996).
[3] T. Vicsek and A. Zafeiris, Phys. Rep. **517**, 71 (2012).
[4] A. Strandburg-Peshkin, C. R. Twomey, N. W. F. Bode, A. B. Kao, Y. Katz, C. C. Ioannou, S. B. Rosenthal, C. J. Torney, H. S. Wu, S. A. Levin, and I. D. Couzin, Curr. Biol. **23**, R709 (2013).
[5] V. N. Tsytovich, Phys.-Usp. **40**, 53 (1997).
[6] M. Chaudhuri, A. V. Ivlev, S. A. Khrapak, H. M. Thomas, and G. E. Morfill, Soft Matter **7**, 1287 (2011).
[7] G. E. Morfill and A. V. Ivlev, Rev. Mod. Phys. **81**, 1353 (2009).
[8] H. J. Keh, Curr. Opin. Colloid Interface Sci. **24**, 13 (2016).
[9] A. V. Ivlev and R. Kompaneets, Phys. Rev. E **95**, 053202 (2017).
[10] R. Kompaneets, G. E. Morfill, and A. V. Ivlev, Phys. Rev. E **93**, 063201 (2016).
[11] C. H. Meredith, P. G. Moerman, J. Groenewold, Y.-J. Chiu, W. K. Kegel, A. van Blaaderen, and L. D. Zarzar, Nat. Chem. **12**, 1136 (2020).
[12] I. Sriram and E. M. Furst, Soft Matter **8**, 3335 (2012).
[13] R. Soto and R. Golestanian, Phys. Rev. Lett. **112**, 068301 (2014).
[14] S. Saha, S. Ramaswamy, and R. Golestanian, New J. Phys. **21**, 063006 (2019).
[15] C. Scheibner, A. Souslov, D. Banerjee, P. Surówka, W. T. M. Irvine, and V. Vitelli, Nat. Phys. **16**, 475 (2020).
[16] M. A. Miri and A. Alù, Science **363**(6422), eaar7709 (2019).
[17] H. Nassar, B. Yousefzadeh, R. Fleury, M. Ruzzene, A. Alù, C. Daraio, A. N. Norris, G. Huang, and M. R. Haberman, Nat. Rev. Mater. **5**, 667 (2020).
[18] J. N. Israelachvili, *Intermolecular and Surface Forces* (Elsevier, Amsterdam, 1992).
[19] M. Dijkstra, R. van Roij, and R. Evans, J. Chem. Phys. **113**, 4799 (2000).
[20] P. G. Bolhuis, A. A. Louis, J. P. Hansen, and E. J. Meijer, J. Chem. Phys. **114**, 4296 (2001).
[21] M. Praprotnik, L. D. Site, and K. Kremer, Annu. Rev. Phys. Chem. **59**, 545 (2008).
[22] B. M. Mognetti, P. Virnau, L. Yelash, W. Paul, K. Binder, M. Müller, and L. G. MacDowell, J. Chem. Phys. **130**, 044101 (2009).
[23] M. E. Cates and J. Tailleur, Annu. Rev. Condens. Matter Phys. **6**, 219 (2015).

[24]C. Bechinger, R. Di Leonardo, H. Löwen, C. Reichhardt, G. Volpe, and G. Volpe, Rev. Mod. Phys. **88**, 045006 (2016).
[25]K. Hayashi and S.-i. Sasa, J. Phys.: Condens. Matter. **18**, 2825 (2006).
[26]M. Durve, A. Saha, and A. Sayeed, Eur. Phys. J. E **41**, 49 (2018).
[27]A. V. Ivlev, J. Bartnick, M. Heinen, C. R. Du, V. Nosenko, and H. Löwen, Phys. Rev. X **5**, 011035 (2015).
[28]J. Agudo-Canalejo and R. Golestanian, Phys. Rev. Lett. **123**, 018101 (2019).
[29]Z. You, A. Baskaran, and M. C. Marchetti, Proc. Natl. Acad. Sci. U. S. A. **117**, 19767 (2020).
[30]S. Saha, J. Agudo-Canalejo, and R. Golestanian, Phys. Rev. X **10**, 041009 (2020).
[31]M. Fruchart, R. Hanai, P. B. Littlewood, and V. Vitelli, Nature **592**, 363 (2021).
[32]S. Saha and R. Golestanian, arXiv:2208.14985 (2022).
[33]S. Osat and R. Golestanian, Nat. Nanotechnol. **18**, 79 (2022).
[34]A. Dinelli, J. O'Byrne, A. Curatolo, Y. Zhao, P. Sollich, and J. Tailleur, arXiv:2203.07757 (2022).
[35]J. Bartnick, M. Heinen, A. V. Ivlev, and H. Löwen, J. Phys.: Condens. Matter **28**, 025102 (2015).
[36]N. P. Kryuchkov, A. V. Ivlev, and S. O. Yurchenko, Soft Matter **14**, 9720 (2018).
[37]A. K. Omar, H. Row, S. A. Mallory, and J. F. Brady, arXiv:2211.12673 (2022).
[38]M. Kumar and C. Dasgupta, Phys. Rev. E **102**, 052111 (2020).
[39]V. Agrawal, V. Pandey, and D. Mitra, arXiv:2206.14172 (2022).
[40]J. A. Anderson, J. Glaser, and S. C. Glotzer, Comput. Mater. Sci. **173**, 109363 (2020).
[41]K. Klymko, P. L. Geissler, J. P. Garrahan, and S. Whitelam, Phys. Rev. E **97**, 032123 (2018).
[42]U. Ray, G. K.-L. Chan, and D. T. Limmer, J. Chem. Phys. **148**, 124120 (2018).
[43]A. Das and D. T. Limmer, J. Chem. Phys. **151**, 244123 (2019).
[44]S. Whitelam, D. Jacobson, and I. Tamblyn, J. Chem. Phys. **153**, 044113 (2020).
[45]U. Ray and G. K.-L. Chan, J. Chem. Phys. **152**, 104107 (2020).
[46]P. Helms and G. K.-L. Chan, Phys. Rev. Lett. **125**, 140601 (2020).
[47]T. H. E. Oakes, A. Moss, and J. P. Garrahan, Mach. Learn. Sci. Technol. **1**, 035004 (2020).
[48]D. C. Rose, J. F. Mair, and J. P. Garrahan, New J. Phys. **23**, 013013 (2021).
[49]A. Das, B. Kuznets-Speck, and D. T. Limmer, Phys. Rev. Lett. **128**, 028005 (2022).
[50]A. J. Schultz and D. A. Kofke, J. Chem. Phys. **149**, 204508 (2018).
[51]S. N. Weber, C. A. Weber, and E. Frey, Phys. Rev. Lett. **116**, 058301 (2016).
[52]C. Hargus, J. M. Epstein, and K. K. Mandadapu, Phys. Rev. Lett. **127**, 178001 (2021).
[53]The low overall density results in these dense liquids occupying little volume, forming spherical droplets within the dilute fluid phase, which comprises most of the system by volume.
[54]E. C. Aifantis and J. B. Serrin, J. Colloid Interface Sci. **96**, 530 (1983).
[55]P. J. Steinhardt, D. R. Nelson, and M. Ronchetti, Phys. Rev. B **28**, 784 (1983).
[56]A. K. Omar, K. Klymko, T. GrandPre, and P. L. Geissler, Phys. Rev. Lett. **126**, 188002 (2021).
[57]We note that our simulation duration (5000τ) limited the periods that we could observe to those with $\tau_{ts} < 2500\tau$, which coincides with $\Delta \geq 1.2$.
[58]J. Stenhammar, R. Wittkowski, D. Marenduzzo, and M. E. Cates, Phys. Rev. Lett. **114**, 018301 (2015).
[59]A. Wysocki, R. G. Winkler, and G. Gompper, New J. Phys. **18**, 123030 (2016).
[60]R. Wittkowski, J. Stenhammar, and M. E. Cates, New J. Phys. **19**, 105003 (2017).
[61]A. K. Omar, Y. Wu, Z.-G. Wang, and J. F. Brady, ACS Nano **13**, 560 (2019).
[62]The diagonal elements of the mutual diffusion tensor are not to be confused with the self-diffusion coefficients computed in this work. The mutual diffusion tensor describes the system response to imposed gradients, and its elements are only equal to self-diffusion coefficients in the dilute limit.
[63]L. Martínez, R. Andrade, E. G. Birgin, and J. M. Martínez, J. Comput. Chem. **30**, 2157 (2009).
[64]A. Stukowski, Model. Numer. Simul. Mater. Sci. **18**, 015012 (2009).
[65]J. D. Weeks, D. Chandler, and H. C. Andersen, J. Chem. Phys. **54**, 5237 (1971).